Optics Communications 454 (2020) 124486

Contents lists available at ScienceDirect

Optics Communications

journal homepage: www.elsevier.com/locate/optcom

A method for assessing the fidelity of optical diffraction tomography reconstruction methods using structured illumination

Ahmed B. Ayoub [a,*], Thanh-an Pham [b], Joowon Lim [a], Michael Unser [b], Demetri Psaltis [a]

[a] Optics Laboratory, Ecole polytechnique fédérale de Lausanne (EPFL), 1015 Lausanne, Switzerland
[b] Biomedical Imaging Group, Ecole polytechnique fédérale de Lausanne (EPFL), CH-1015 Lausanne, Switzerland

ARTICLE INFO

Keywords:
Optics
Structured illumination
Optical tomography
3D refractive index reconstructions
Biological samples

ABSTRACT

A fundamental challenge in 3D tomographic reconstruction is the difficulty of obtaining ground truth about test objects with which to assess the fidelity of the 3D reconstruction. We present a method that provides such a quantitative metric of the accuracy of the three dimensional reconstruction for optical tomography. The method relies on spatial light modulation of the illumination beam through the sample and numerical back-propagation of the phase conjugated experimentally measured optical field through the 3D reconstruction of the object. The fidelity of this reconstruction provides a quantitative measure of the accuracy of the 3D reconstruction without direct access to the ground truth about the 3D object.

1. Introduction

Light microscopy plays an important role in many fields and especially in label-free detection and characterization of microstructures and biological cells/specimens which becomes a primary goal for biomedical applications. Optical Diffraction Tomography (ODT) is an example of such quantitative characterization of biological specimens by reconstructing the 3D refractive index (RI). Several reconstruction methods have been employed for the RI reconstruction [1–20]. Since ODT does not require staining, it can be used in various biological studies including immune cells [21], red blood cells [22], and embryos [23]. ODT images are formed by first recording the complex field of projections taken at different illumination angles. Excluding digital phantoms and samples for which we have a-priori knowledge (i.e. 3D printed samples), we generally lack information about the ground truth of 3D samples. This lack of information becomes particularly serious in biomedical applications since accurate characterization is necessary for diagnosis and cure. For example, in cellular imaging, this lack of information leads to uncertainty in the calculation of the RI of the sample which is interrelated to the protein concentration inside the cells. One way to quantify this uncertainty is through the use of phantom objects such as beads or microspheres. However, this way cannot be generalized to biological samples since their ground truth is not available.

In this paper we describe and experimentally demonstrate a method that provides a comparative metric for assessing the relative performance of reconstruction algorithms for arbitrary 3D objects without having access to their ground truth. To do this, digital phase conjugation and back-propagation through inhomogeneous media were used. The distortion imposed on an optical field propagating through an inhomogeneous medium with negligible absorption can be undone if the transmitted field is holographically recorded and the phase conjugate reconstruction of the hologram is made to propagate backwards through the sample [24–27]. This is conveniently done in the optical domain by illuminating the recorded hologram with a plane wave counter-propagating to the plane wave used to record the hologram. When the incident beam illuminating the object is spatially modulated by a 2D pattern (an image), the field arriving at the hologram plane is a distorted version of the 2D illumination pattern. Through phase conjugation, this distortion is removed and the field arriving back at the input plane is ideally an exact replica of the original image. Deviations from this ideal condition can occur due to limited spatial bandwidth, absorption or other losses in the optical path. Any imperfection in the holographic recording and play-back of the hologram (including speckle) can also contribute to deviations of the phase conjugate reconstruction from the original image projected through the sample. In a carefully designed optical system in which the coherent noise is minimal (i.e. due to dust particles or multiple reflections from optical elements), we can generally obtain excellent phase conjugate reconstructions since the medium where the beam propagates through is well defined. The phase conjugate image is also strongly affected by any changes in the 3D object in the time between the recording of the hologram and the play-back. If the effect of noise is negligible, then any distortions in the phase conjugate image can be attributed to changes in the object itself. This effect has been used for many applications including imaging through diffusing media [24], turbidity suppression in biological samples [25,26] and imaging through turbid media [27].

* Corresponding author.
E-mail address: ahmed.ayoub@epfl.ch (A.B. Ayoub).

https://doi.org/10.1016/j.optcom.2019.124486
Received 27 June 2019; Received in revised form 20 August 2019; Accepted 27 August 2019
Available online 3 September 2019

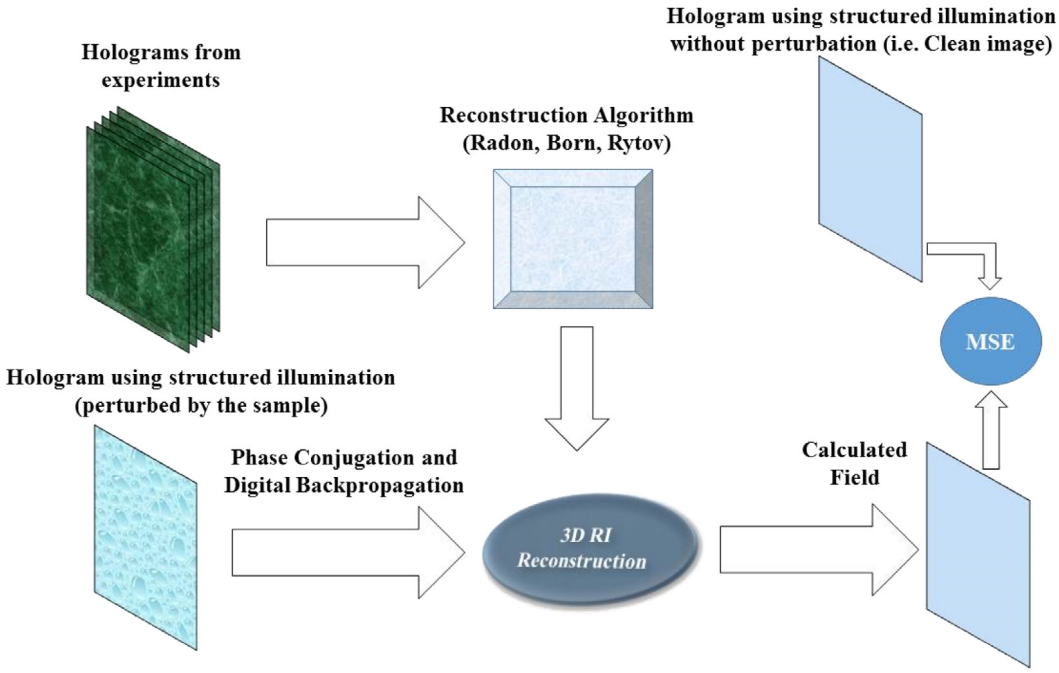

Fig. 1. The overall scheme of the proposed assessment technique.

In this paper we use this effect to assess the accuracy of the estimate of a 3D reconstruction.

Fig. 1 shows the overall idea behind the proposed assessment technique. First, different holograms from different illumination angles of the 3D object are recorded on a sCMOS camera using the experimental setup that is described below. Using this information, we can reconstruct the 3D refractive index map using well known algorithms (i.e. Radon [10], Born [1] and Rytov [4–6]). On the same setup, we illuminate a known pattern onto the sample with structured illumination by recording a pattern on the spatial light modulator (SLM). The pattern gets distorted by the 3D sample as it propagates through the 3D sample along the optical path. Phase conjugation of the distorted pattern is performed digitally by computationally propagating the conjugate of the experimentally measured field through the 3D object whose index distribution has been estimated using the above mentioned algorithms. Using accurate digital wave propagation and assuming perfect 3D reconstruction, we expect a faithful digital reconstruction of the pattern that was presented on the SLM. Distortions in the digital reconstruction of the 2D pattern that was placed on the SLM are partially due to inaccuracies of the 3D reconstruction algorithm. Measurement of the degree of distortion in the digital reconstruction of the SLM pattern provides a quantitative metric which we can use to compare ODT reconstruction algorithms.

The three commonly used reconstruction algorithms were tested: Radon [10], Born [1] and Rytov [4–6]. Comparisons between Born and Rytov have been performed in literature in different optical regimes [28,29]; however, such studies cannot directly be translated to arbitrary sharped samples such as biological samples. The proposed method in the paper can work as a good reconstruction assessment tool for any other reconstruction method [19–31]. The goal of this paper is to present the assessment method and therefore we did not include a comprehensive comparison of the entire set of reconstruction algorithms.

2. Materials and methods

2.1. Experimental set-up and samples

The optical system shown in Fig. 2 used a diode pumped solid state (DPSS) 532 nm laser. The laser beam was first spatially filtered using a pinhole. A beam-splitter separated the input beam into a signal and a reference beam in an off-axis geometry. The signal beam was directed to the sample at different angles of incidence using a reflective liquid crystal on silicon (LCOS) spatial light modulator (SLM) (Holoeye PLUTO VIS, pixel size: 8 μm, resolution: 1080×1920 pixels) that modulates the phase of the incident beam. Different illumination angles were obtained by displaying blazed gratings on the SLM. In the experiments presented here, a blazed grating with a period of 25 pixels (200 μm) was rotated a full 360° with a resolution of 1 degree for a total of 361 projections, including normal incidence to be able to measure the shift of the k vectors with respect to it. Two 4f systems between the SLM and the sample permitted filtering of higher orders reflected from the SLM (due to the pixilation of the device) as well as 240x angular magnification of the SLM projections onto the sample. Using a 100X oil immersion objective lens (OBJ1) with NA 1.4 (Olympus), the incident angle on the sample corresponding to the 200 μm grating was about 37°. A third 4f system after the sample includes a 100X oil immersion objective lens (OBJ2) with NA 1.45 (Olympus). The sample and reference beams were collected on a second beam-splitter and projected onto a scientific complementary metal-oxide-semiconductor (sCMOS) camera (Andor Neo 5.5 sCMOS, pixel size: 6.5 μm, resolution: 2150 × 2650 pixels). The samples used were HCT-116 human colon cancer cells and Panc-1 human pancreas cancer cells which were cultured in McCoy 5A growth medium (Gibco) supplemented with 10% fetal bovine serum (Gibco). #1 coverslips were treated with a 5 μg/mL solution of fibronectin (Sigma) in phosphate-buffered saline (PBS) and let to dry at room temperature. Cells at passage 18 were removed from culture flasks using trypsin, seeded directly onto the fibronectin-treated coverslips, and incubated 24 h in a 37C/5% CO2 atmosphere until cells adhered and spread on the coverslips. Each sample was fixed for 10 min at room temperature in 4% paraformaldehyde in PBS, rinsed twice with PBS, and sealed with a second coverslip.

2.2. Propagation model

To ensure accurate propagation through inhomogeneous medium, we used the Lippmann–Schwinger Equation (LSE) [32,33]. The Lippmann–Schwinger equation is the same as the integral equation

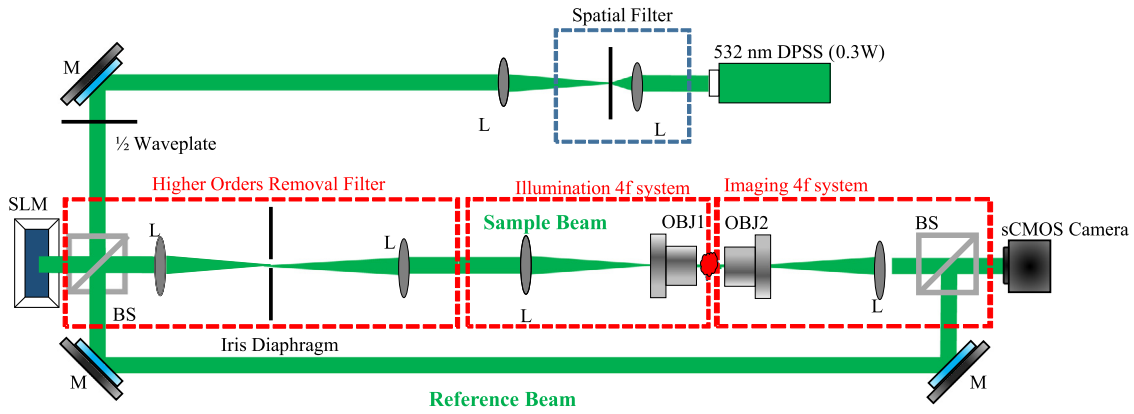

Fig. 2. Experimental tomographic setup. (M: Mirror, L: Lens, OBJ: Objective lens, BS: Beam splitter). Pinhole-based spatial filter cleans out the beam spatially. The Higher orders cleaning filter removes the unneeded higher orders that might interfere at the image plane on the sample causing image deterioration.

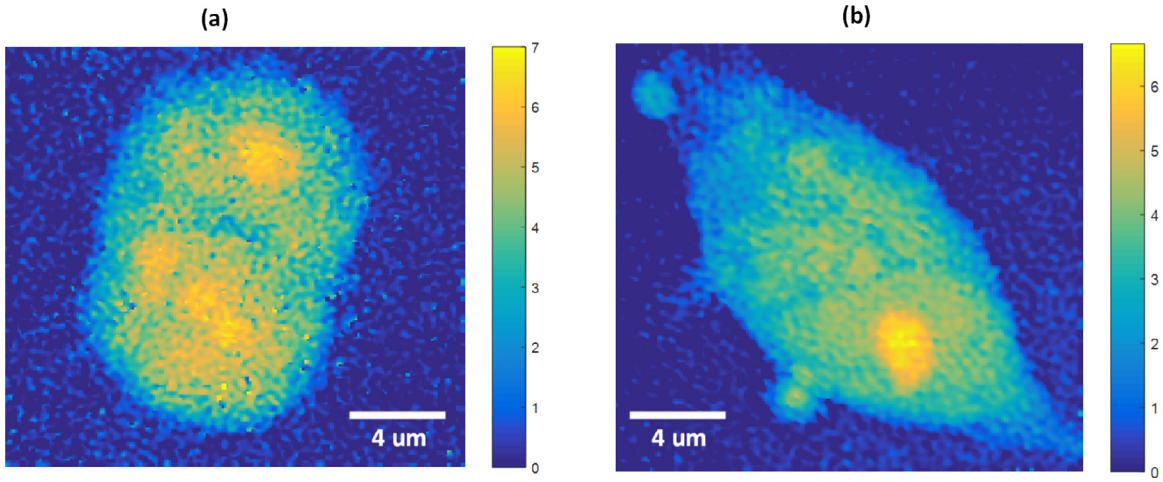

Fig. 3. Unwrapped phase of (a) HCT-116 cell and (b) Panc-1 cell for normal incidence. Phase unwrapping was done using PUMA algorithms. Color bars are in Radians.

described in Born and Wolf [34]. This integral equation is formulated as follows

$$E(r) = E_{inc}(r) + \int G(r - r')E(r')\eta(r')dr',$$

where E_{inc} and E are the incident and total field respectively of wavelength λ. G(r) denotes the Green function, $\eta(r) = k^2\left(\frac{n(r)^2}{n_m^2} - 1\right)$ is the scattering cross-section of the sample of refractive index $n(r)$, with $k = 2\pi n_m/\lambda$ the optical wavenumber in the medium of refractive index n_m. Our numerical propagation is divided in two sequential steps:

$$E = (I - G\eta)^{-1} E_{inc} \quad (1)$$

$$E^{meas} = G^{meas}(E\eta) + E_{inc}^{meas}, \quad (2)$$

where η, E_{inc} denote the scattering cross-section of the sample and the incident field discretized in the region of interest (i.e., which includes the sample), and G denotes the discrete convolution with the Green function. Similarly, G^{meas} denotes the discrete convolution with the Green function that gets the scattered field at the sensors position and E_{inc}^{meas} is the incident field at the sensors position. In Eq. (1), we compute the discrete total field E in the region of interest by inverting a matrix. In this work, we use the BiConjugate Gradients Stabilized Method to iteratively compute the matrix inverse [35]. In Eq. (2), E^{meas} refers the total field at the sensor positions. The LSE method is very accurate since beyond the scalar assumption, there is no further approximation. The multiple scattering events (including reflections) are fully accounted for as opposed to the beam propagation method.

2.3. Tomographic reconstruction methods

For 3D RI reconstruction, three computational techniques were considered; Radon, Born, and Rytov. ODT was first described by Wolf [1,2] and refined by Devaney [6]. Like the first order Born approximation, the first order Rytov approximation is also a linearization of the inverse scattering problem but it has been found to yield superior results for biological cells and has been the most commonly used technique for linear ODT [6–20]. One of the main differences between the Rytov and the Born models is the phase unwrapping that is explicit in the Rytov model [36]. This unwrapped phase is used instead of the field in the inversion formula introduced by Wolf (which we refer to as the Wolf transform). The third technique, the Radon direct inversion based reconstruction [10], is a filtered back-projection reconstruction algorithm that is based on diffraction-free model thus it generates errors when it comes to diffracting objects with spatial variations comparable to the wavelength of light. A phase unwrapping algorithm was used to unwrap the phase [37] of the holographically recorded projections. Two examples of such projections are shown in Fig. 3. In the studied samples (i.e. HCT-116 cells and Panc-1 cells), the accumulated phase from the samples, whose thickness is around 8 μm, exceeds 2π at some regions depending on the proteins distributions as shown in Fig. 3a, b. Both Radon and Born fail to reconstruct the 3D refractive index distribution due to considerable diffraction, and high phase accumulation by the sample, respectively. Slices in x-y and x-z of the 3D reconstructions of the two cells are shown in Fig. 4. Notice that the methods based on the Born and Rytov approximations are significantly different in estimating the refractive index distribution.

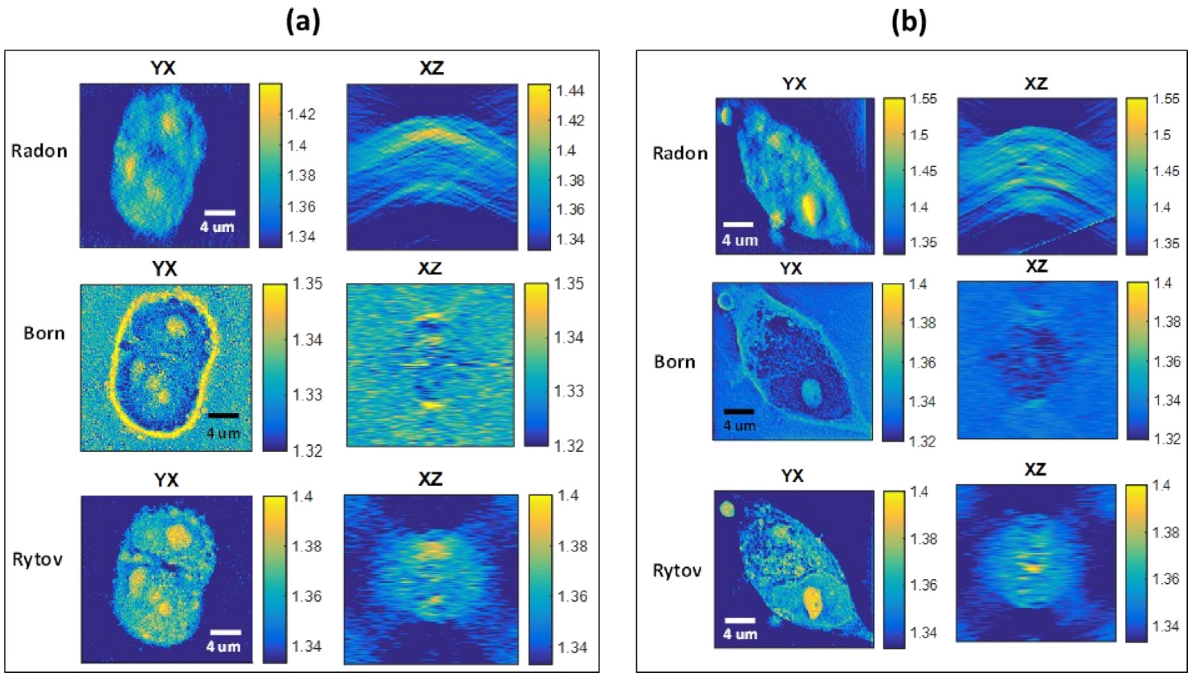

Fig. 4. 3D reconstruction based on Radon, Born, and Rytov techniques for (a) HCT-116 cell and (b) Panc-1 cell.

Cancer cells usually have a RI of cytoplasm that range between 1.36–1.39 due to excess RNA and protein [7]. As observed in Fig. 4a, this index range is probably under-estimated (i.e. around 1.32) due to high phase delay that Born cannot deal with. On the contrary, the Rytov approximation shows better agreement with what is expected from the biology of cells. The estimated index of the cytoplasm is around 1.365 which is within the expected range. Another interesting feature is the lipids which are composed of fats, sugars and proteins and are characterized by their high proteins concentrations and thus high RI value. This is in agreement with the Rytov reconstructions where we can see bright spots which do not show up in the Born approximation [7]. In Fig. 4b, it is obvious how the Born under-estimates the RI value of the nucleus as well where it should have much higher RI than the surrounding media (i.e., water) [7]. This could be because phase unwrapping is not considered and that is why we can see enhanced edges at the boundaries of the cell at the point where the phase wraps while the higher phase is under estimated. In addition the RI contrast between nucleus and medium is quite low in case of Born. On the other hand, Rytov agrees with literature where the high RI contrast is clear [7,38–40].

3. Assessment results

We quantitatively assess the performance of each of the three reconstruction methods (i.e. Radon, Born, and Rytov) in the same experimental setup using digital phase conjugation method as described earlier. First we illuminated the 3D sample with a phase modulated beam with an image of Einstein or the 1951 USAF resolution test chart that are displayed on the SLM. The phase modulated beam that comes through the sample is holographically recorded on the sCMOS camera. The wrapped phase of such an image is shown in Fig. 5. Structured illumination was used instead of plane waves since structured illumination by its own can be thought of as many plane waves propagating at the same time and hence probe a larger portion of the 3D spectrum of the object. In addition, assessment using structured illumination ensures fairness as these patterns were not used in the tomographic reconstruction. In order to measure the incident field, we repeat the exact same measurement by propagating through the media (clear PBS liquid between two coverslips). We consider the measurement we obtain from this step as the "Original" pattern since there is minimal distortion along the optical path. The second step in the assessment is done computationally by back-propagating the modulated output (i.e. picture of Einstein or the USAF resolution test chart modulated with the HCT-116/Panc-1 phase delay) through the reconstructed 3D refractive index (RI) map. We use the Lippmann–Schwinger Equation (LSE) propagation model described above [32,33]. The LSE method requires a larger memory and longer processing time (as compared to the beam propagation method [41] where reflections are neglected) however this method is more accurate. From these two steps, we expect an accurate refractive index reconstruction to result in a clean reconstruction of the original structured illumination pattern. Comparison with the original pattern measured from the experiment without the cell gives us a quantitative measure of the accuracy of the ODT method. Fig. 6 shows the retrieved Einstein and 1951 USAF resolution test chart for the case of Radon, Born, and Rytov approximations as compared to the original field using this procedure.

Table 1
MSE percentage for Radon, Born and Rytov based reconstruction techniques for Einstein.

Radon	Born	Rytov
8.83%	34.73%	6.39%

To quantify the error, the mean square error (MSE) between the measured and retrieved fields is calculated. Assessment was done for reconstructions provided by Radon, Born, and Rytov approximations as shown in Tables 1 and 2. The MSE in the case of Born reconstruction is high as compared to Radon and Rytov (at least 3 times higher than MSE for Rytov). This is due to the fact that both Radon and Rytov make use of the unwrapped phase whereas the Born reconstruction algorithm is implemented on the complex field. The Radon reconstruction scheme depends on the unwrapped phase; however it ignores diffraction which limits its performance as compared to Rytov which have the best performance by taking into account phase unwrapping, and diffraction.

Although the MSE values are changing from one case to another (depending on phase profile, dimensions and diffraction strength), the three reconstructions follow the same trend where Born has the worst performance as compared to Radon and Rytov.

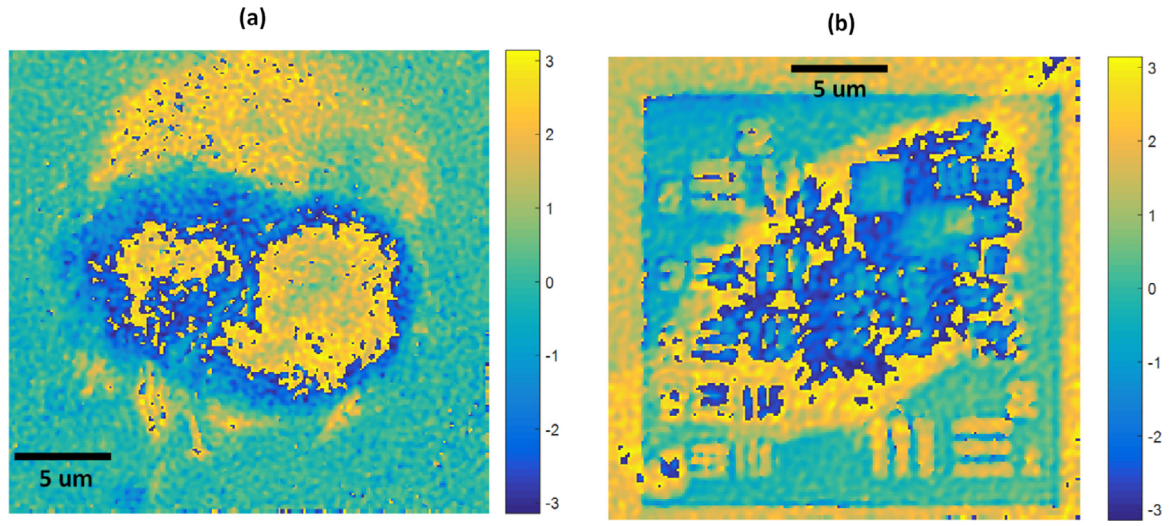

Fig. 5. Wrapped phase of Einstein/USAF chart after propagating through the HCT-116/Panc-1 cell.

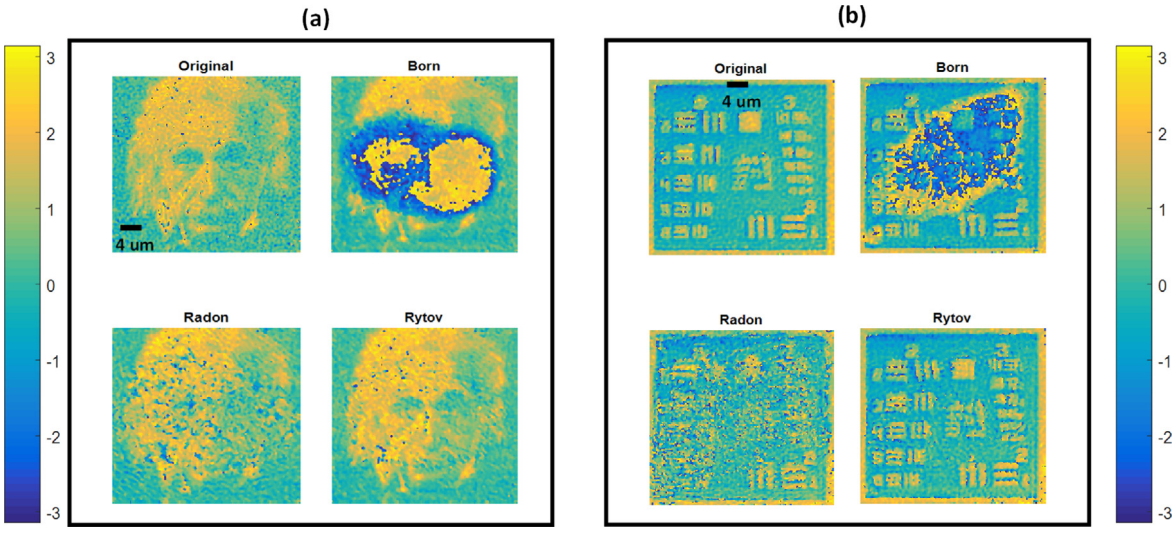

Fig. 6. Retrieved projected fields using Radon, Born, and Rytov for (a) Einstein through HCT-116 cell, and (b) USAF chart through Panc-1 cell.

Table 2
MSE percentage for Radon, Born and Rytov based reconstruction techniques for USAF chart.

Radon	Born	Rytov
16.19%	24.58%	7.97%

4. Conclusion

We showed how structured illumination can be used to assess the performance of different reconstruction schemes through the use of an SLM for both angular scanning and structured illumination. Having the same experimental setup for angular and structured illumination without the burden of alignment and/or mechanical instabilities, it is possible to evaluate the performance of the different reconstruction algorithms by quantifying the error between different reconstructions based on the retrieved field from the digitally back-propagated output field recorded on the detector using the LSE. This assessment method is useful when imaging biological samples where the ground-truth cannot be known while the reconstructions need to be validated. The method we present is applicable to any 3D reconstruction technique that provides an estimate of the 3D index distribution of the sample. A complete assessment for the entire reconstruction algorithm is considered for future work.

References

[1] E. Wolf, Three-dimensional structure determination of semi-transparent objects from holographic data, Opt. Commun. 1 (4) (1969) 153.
[2] E. Wolf, Determination of the amplitude and the phase of scattered fields by holography, J. Opt. Soc. Amer. 60 (1970) 18–20.
[3] Florian Charrière, Anca Marian, Frédéric Montfort, Jonas Kuehn, Tristan Colomb, Etienne Cuche, Pierre Marquet, Christian Depeursinge, Cell refractive index tomography by digital holographic microscopy, Opt. Lett. 31 (2006) 178–180.
[4] F. Merola, P. Memmolo, L. Miccio, R. Savoia, M. Mugnano, A. Fontana, G. D'Ippolito, A. Sardo, A. Iolascon, A. Gambale, P. Ferraro, Tomographic flow cytometry by digital holography, Light: Sci. Appl. 6 (2017) e16241.
[5] K. Lee, K. Kim, J. Jung, J. Heo, S. Cho, S. Lee, G. Chang, Y. Jo, H. Park, Y. Park, Quantitative phase imaging techniques for the study of cell pathophysiology: From principles to applications, Sensors 13 (4) (2013) 4170–4191.
[6] A.J. Devaney, Mathematical Foundations of Imaging and Tomography and Wavefield Inversion, Cambridge Univ. Press, 2012.
[7] O. Haeberle, K. Belkebir, H. Giovaninni, A. Sentenac, Tomographic diffractive microscopy: basics, techniques and perspectives, J. Modern Opt. 57 (9) (2010) 686–699.
[8] W. Choi, et al., Tomographic phase microscopy, Nat. Methods 4 (9) (2007) 717–719.

[9] Y. Sung, W. Choi, N. Lue, R.R. Dasari, Z. Yaqoob, Stain-free quantification of chromosomes in live cells using regularized tomographic phase microscopy, PLoS One 7 (11) (2012) e49502.
[10] J. Radon, Uber die bestimmung von funktionen durch ihre integralwerte langs gewisser mannigfaltigkeiten, Ber. Sachs. Akad. Wiss. 69 (1917) 262–277.
[11] D. Huang, et al., Optical coherence tomography, Science 254 (5035) (1991) 1178–1181.
[12] T.S. Ralston, D.L. Marks, P.S. Carney, S.A. Boppart, Real-time interferometric synthetic aperture microscopy, Opt. Express 16 (4) (2008) 2555–2569.
[13] G. Popescu, Quantitative Phase Imaging of Cells and Tissues, McGraw Hill, 2011.
[14] D. Gabor, A new microscopic principle, Nature 161 (1948) 777.
[15] F. Zernike, Phase contrast a new method for the microscopic observation of transparent objects, part 1, Physica 9 (7) (1942) 686–698.
[16] M. Mir, et al., Visualizing escherichia coli sub-cellular structure using sparse deconvolution spatial light interference tomography, PLoS One 7 (6) (2012) e39816.
[17] T. Kim, et al., White-light diffraction tomography of unlabelled live cells, Nature Photon. 8 (3) (2014) 256–263.
[18] H.F. Ding, Z. Wang, F. Nguyen, S.A. Boppart, G. Popescu, Fourier transform light scattering of inhomogeneous and dynamic structures, Phys. Rev. Lett. 101 (23) (2008) 238102.
[19] J. Kostencka, T. Kozacki, A. Kuś, B. Kemper, M. Kujawińska, Holographic tomography with scanning of illumination: space-domain reconstruction for spatially invariant accuracy, Biomed. Opt. Express 7 (2016) 4086–4101.
[20] Y.J. Sung, et al., Optical diffraction tomography for high resolution live cell imaging, Opt. Express 17 (1) (2009) 266–277.
[21] J. Yoon, K. Kim, H. Park, C. Choi, S. Jang, Y. Park, Label-free characterization of white blood cells by measuring 3D refractive index maps, Biomed. Opt. Express 6 (10) (2015) 3865–3875.
[22] Y. Kim, H. Shim, K. Kim, H. Park, S. Jang, Y. Park, Profiling individual human red blood cells using common-path diffraction optical tomography, Sci. Rep. 4 (2014) 6659.
[23] T.H. Nguyen, M.E. Kandel, M. Rubessa, M.B. Wheeler, G. Popescu, Gradient light interference microscopy for 3D imaging of unlabeled specimens, Nat. Commun. 8 (1) (2017) 210.
[24] E.N. Leith, J. Upatnieks, Holographic imagery through diffusing media, J. Opt. Soc. Amer. A 56 (1966) 523.
[25] Z. Yaqoob, D. Psaltis, M. Feld, C. Yang, Optical phase conjugation for turbidity suppression in biological samples, Nat. Photon. 2 (2008) 110.
[26] M. Cui, C. Yang, Implementation of a digital optical phase conjugation system and its application to study the robustness of turbidity suppression by phase conjugation, Opt. Express 18 (2010) 3444–3455.
[27] C.L. Hsieh, Y. Pu, R. Grange, G. Laporte, D. Psaltis, Imaging through turbid layers by scanning the phase conjugated second harmonic radiation from a nanoparticle, Opt. Express 18 (2010) 20723–20731.
[28] D. Tajik, A.D. Pitcher, N.K. Nikolova, Comparative study of the rytov and Born approximations in quantitative microwave holography, Prog. Electromagn. Res. B 79 (2017) 1–19, http://dx.doi.org/10.2528/PIERB17081003.
[29] D. Tajik, D.S. Shumakov, N.K. Nikolova, An experimental comparison between the born and rytov approximations in microwave tissue imaging, in: 2017 IEEE MTT-S International Microwave Symposium (IMS), Honolulu, HI, 2017, pp. 1391–1393, http://dx.doi.org/10.1109/MWSYM.2017.8058875.
[30] Joowon Lim, Alexandre Goy, Morteza H. Shoreh, Michael Unser, Demetri Psaltis, Learning tomography assessed using mie theory, Phys. Rev. Appl. 9 (2018) 034027.
[31] M.H. Shoreh, A. Goy, J. Lim, U. Kamilov, M. Unser, D. Psaltis, Optical tomography based on a nonlinear model that handles multiple scattering, in: 2017 IEEE International Conference on Acoustics, Speech and Signal Processing (ICASSP), New Orleans, LA, 2017, pp. 6220–6224.
[32] H. Liu, D. Liu, H. Mansour, P.T. Boufounos, L. Waller, U.S. Kamilov, SEAGLE: Sparsity-driven image reconstruction under multiple scattering, IEEE Trans. Comput. Imaging 4 (1) (2018) 73–86.
[33] Emmanuel Soubies, Thanh-An Pham, Michael Unser, Emmanuel soubies thanh-an pham michael unser efficient inversion of multiple-scattering model for optical diffraction tomography, Opt. Express 25 (2017) 21786–21800.
[34] M. Born, E.W. Wolf, Principles of Optics, 7th edition, Cambridge University, 2001, pp. 104–105.
[35] H.A. van der Vorst, Bi-CGSTAB: A fast and smoothly converging variant of bi-CG for the solution of nonsymmetric linear systems, SIAM J. Sci. Stat. Comput. 13 (2) (1992) 631–644.
[36] M. Slaney, A.C. Kak, L.E. Larsen, Limitations of imaging with first-order diffraction tomography, IEEE Trans. Microw. Theory Tech. 32 (8) (1984) 860–874.
[37] J.M. Bioucas-Dias, G. Valadão, Phase unwrapping via graph cuts, IEEE Trans. Image Process. 16 (3) (2007) 698–709.
[38] K. Haseda, K. KAnematcu, K. Noguchi, H. Saito, N. Umeda, Y. Ohta, Significant correlation between refractive index and activity of mitochondria: single mitochondrion study, Biomed. Opt. Express 6 (3) (2015) 859–869.
[39] J.D. Wilson, W.J. Cottrell, T.H. Foster, Index-of-refraction-dependent subcellular light scattering observed with organelle-specific dyes, J. Biomed. Opt. 12 (1) (2007) 014010.
[40] J.A. Valkenburg, C.L. Woldringh, Phase separation between nucleoid and cytoplasm in escherichia coli as defined by immersive refractometry, J. Bacteriol. 160 (3) (1984) 1151–1157.
[41] J. Van Roey, J. van der Donk, P.E. Lagasse, Beam-propagation method: analysis and assessment, J. Opt. Soc. Amer. 71 (1981) 803–810.